Capture and ionization in laser-assisted proton–hydrogen collisions

Thomas Niederhausen* and Uwe Thumm[†]

James R. Macdonald Laboratory, Kansas State University, Manhattan, Kansas 66506-2604, USA

(Received 2 December 2005; published 14 April 2006)

We calculate electron capture and ionization probabilities for ion–atom collisions in a strong laser field $(5 \times 10^{13} \text{ W/cm}^2)$ by numerically solving the three-dimensional time-dependent Schrödinger equation. For circularly polarized laser fields and an impact energy of 1.2 keV/amu, we find a substantial modification of the electronic dynamics in the H^+–H collision system as compared to field-free collisions. In particular, we observe a strong dependence on the initial laser phase and the impact parameter for both capture and ionization, which can be explained using semiclassical arguments.

Driven by laser systems with increasing intensities and improving control, and refined techniques for the momentum-resolved detection of ions, atoms, and photoemitted electrons, interactions of intense laser fields with atoms and molecules continue to attract attention [1–4]. Ever since the invention of the laser, the challenge to efficiently control chemical reaction pathways with laser light has remained attractive for both fundamental and applied research. Electron emission and transfer processes have been studied in ion-atom collisions for many decades and have significantly contributed to our understanding of electronic dynamics in complex, three- (or more) body Coulomb systems. However, laser-assisted ion-atom collisions, in which charge transfer and ionization processes of an ordinary collision reaction are modified due to the presence of an intense external electromagnetic field, have emerged only very recently [5–11] as a new line of research that promises to combine the benefits of atomic collision studies (e.g., the improved understanding of chemical reactions) and laser physics (control). It has been shown theoretically that the proper choice of the laser parameters leads to significantly enhanced electron capture [5], modification of ionization probabilities [6], ponderomotively shifted emission of binary-encounter electrons in fast collisions [9], and generation of ultrahigh harmonics of the fundamental laser frequency [11].

While laser-assisted electron-atom collisions [3,12–14] have been investigated theoretically and experimentally for more than one decade, so far no experiments have been carried out for laser-assisted ion-atom encounters. This is due to the challenging task of intersecting—in space and time—a strong laser pulse with the ion-atom interaction, while discriminating the laser-assisted events from the field-free collisions. However, recently improved momentum spectroscopy methods [15,16] in combination with currently being developed picopulsed ion beams [17] and new experiments with ns ion beams [18] may soon provide experimental data. Theoretically, laser-assisted collisions have been described within basis-set expansions (atomic two-state approximations [19], adaptive basis generator calculations [5]), pertur-

bative calculations [6], and grid-based methods [7,8,11].

In this Communication, we investigate the laser-assisted collision between a 1.21-keV proton and a hydrogen-atom target, exposed to a circularly polarized laser field of $5 \times 10^{13} \text{ W/cm}^2$ intensity (Fig. 1). The presence of the laser breaks the cylindrical symmetry of the $p+\text{H}(1s)$ collisions and allows us to distinguish the following special cases: (i) *corotating* collisions, where the impact angle α (Fig. 1) is zero, and the angular momentum of the projectile $\mathbf{L}=\mathbf{R} \times m_p \mathbf{v}$, is parallel to the helicity vector $\mathbf{h}$ of the laser (in other words, the projectile rotation around the target nucleus follows the same direction as the rotating laser-electric field); (ii) *counterrotating* collisions with $\alpha=180°$ where $\mathbf{L}$ and $\mathbf{h}$ are antiparallel (referring to a rotation of the projectile around the target in opposite direction as the rotation of the laser-electric field); and (iii) *off-plane* collisions with $\alpha=\pm 90°$ where the internuclear axis is perpendicular to the plane of the laser-electric field at the time of closest approach.

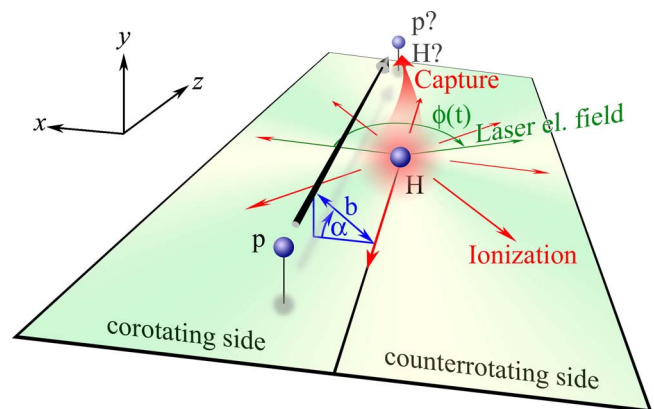In the length form and in dipole approximation the Hamiltonian for the collision system is

FIG. 1. (Color online) Scenario of the collision between a moving proton and a hydrogen atom, characterized by the impact parameter b and the angle α with the xz plane in which the laser electric field rotates. The overall laser phase $\phi=\phi(t_0)$ is the direction of the electric field at the time $t=t_0$ of closest approach.

*Electronic address: esdimax@phys.ksu.edu

[†]Electronic address: thumm@phys.ksu.edu

TABLE I. Comparison of the total capture cross sections for field-free collisions. Results for 3D and 2D grid calculations, basis-set (END) calculations, and experimental data.

Source	σ_{tot} (10^{-15} cm^2)
3D grid	19.0
2D model[a]	21.9
END method[b]	16.3
experiment[c]	15.6±18%

[a]Reference [8].
[b]Reference [25].
[c]Reference [24].

$$\hat{H}(t) = -\frac{1}{2}\nabla^2 - \frac{1}{r} - \frac{1}{|\mathbf{r} - \mathbf{R}(t)|} + \mathbf{r} \cdot \mathbf{E}(t), \qquad (1)$$

where $\mathbf{R}(t)=(b\cos\alpha, b\sin\alpha, vt)$ denotes the projectile trajectory in straight-line approximation with projectile velocity v, impact parameter b, and impact angle α relative to the xz plane (we use atomic units throughout, unless stated otherwise). The circularly polarized electric field of the laser radiation is confined to the xz plane,

$$\mathbf{E}(t) = E_0(t)(\cos[\omega t + \phi], 0, \sin[\omega t + \phi]). \qquad (2)$$

$E_0(t)$ is the envelope function and ϕ the laser phase at the time ($t=0$) of closest approach between projectile and target. We assume that the laser pulse has been ramped adiabatically to the constant electric-field amplitude E_0 long before the collision takes place.

We solve the time-dependent Schrödinger equation on a three-dimensional (3D) grid, using the Crank-Nicholson propagation scheme [20–22]. We use equal grid spacings in all three coordinate directions $\Delta x = \Delta y = \Delta z = 0.25$ for a grid that covers 80 a.u. in the z direction and a length of at least 60 a.u. in the x and y directions, adjusted depending on the value of b. We employ an absorbing optical potential to suppress nonphysical effects due to reflections of the electronic wave function at the grid boundaries [8] and introduce a small soft-core parameter to the nuclear potential to avoid the Coulomb singularities at the nuclei [23].

We tested our numerical scheme for field-free collisions and found total (angle-integrated) capture cross sections in agreement with experimental data [24], while our b-dependent capture probabilities are in fair agreement with the electron–nuclear dynamics approach (END) [25]. Our full 3D calculations lead to about 15% smaller total capture cross sections than previous two-dimensional (2D) reduced dimensionality results [8] and therefore constitute a significant quantitative improvement (Table I).

In our laser-assisted calculations, we choose the wavelength 1064 nm of a Nd:YAG laser, corresponding to the frequency $\omega=0.044$. For a typical impact parameter of $b=1$, Fig. 2 shows the dependence of the electron capture probability on the absolute laser phase ϕ at the time of closest approach. Maxima appear at $\phi=90°$ and $\phi=270°$, when the force of the laser electric field at the time of closest approach is either parallel or antiparallel to the motion of the projec-
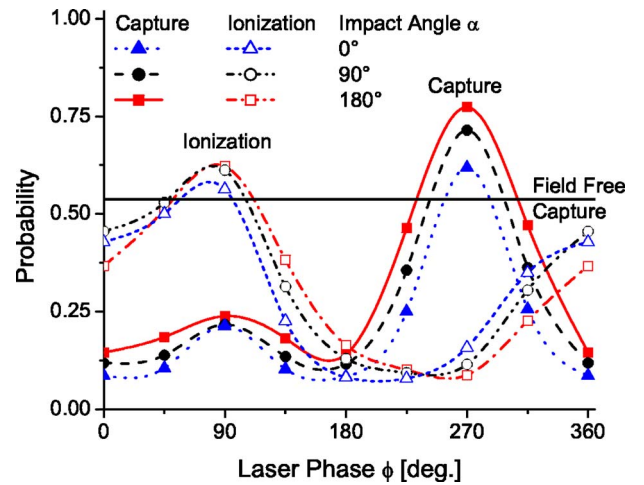

FIG. 2. (Color online) Laser-phase dependence of the electron capture and ionization probabilities at fixed impact parameter $b=1$ for three different impact angles α. Also shown is the field-free capture probability. Field-free ionization probability is negligible.

tile. This agrees with an energy matching argument: Resonant capture occurs predominantly, when the electronic energies of the laser-dressed projectile and target states are identical, i.e., when the laser-electric-field vector is perpendicular to the internuclear axis. Clearly, the time interval during which level matching near the point of closest approach can approximately be maintained is larger for corotating than for counterrotating collisions. For the projectile speed and impact parameter in Fig. 2, the collision time is of the order of half a laser cycle (≈ 71.4 a.u.), while the electronic time scale is about two orders of magnitude faster (≈ 1 a.u.). This enables the transient formation of a molecular state, even for counterrotating collisions where the matching condition only holds for a small fraction of one laser cycle. In contrast, for corotating collisions, level matching is maintained much longer and for approximately 1/2 of a laser cycle. For the given parameters this favors recapture by the target and explains that the capture cross sections in Fig. 2 are smaller for corotating collisions. The phase dependence of the electron capture probability near $\phi=90°$ is broadened for counterrotating as compared with off-plane collisions at $\alpha=\pm 90°$. For corotating collisions, in contrast, the capture probability changes faster near $\phi=90°$ than for $\alpha=\pm 90°$ off-plane collisions.

For $b=1$, the ionization probability has a maximum at $\phi=90°$ (Fig. 2). At this laser phase, the laser electric force $\mathbf{F}_L(t=0)$ on the electron at the time of closest approach is antiparallel to the projectile velocity $\mathbf{v}$, thereby reducing the chance for electron capture and recapture. In contrast, near $\phi=270°$, $\mathbf{F}_L(t\approx 0)$ is nearly parallel to $\mathbf{v}$ and facilitates capture. This effect explains relatively small ionization and large capture probabilities near $\phi=270°$.

In Figs. 3(a)–3(c) the dependence of the electron capture probability on both the impact parameter b and the laser phase ϕ is shown for the three cases: corotating [Fig. 3(a)], off-plane with $\alpha=\pm 90°$ [Fig. 3(b)], and counterrotating [Fig. 3(c)] collisions. This graph exhibits the features discussed above for fixed impact parameters, namely enhanced capture
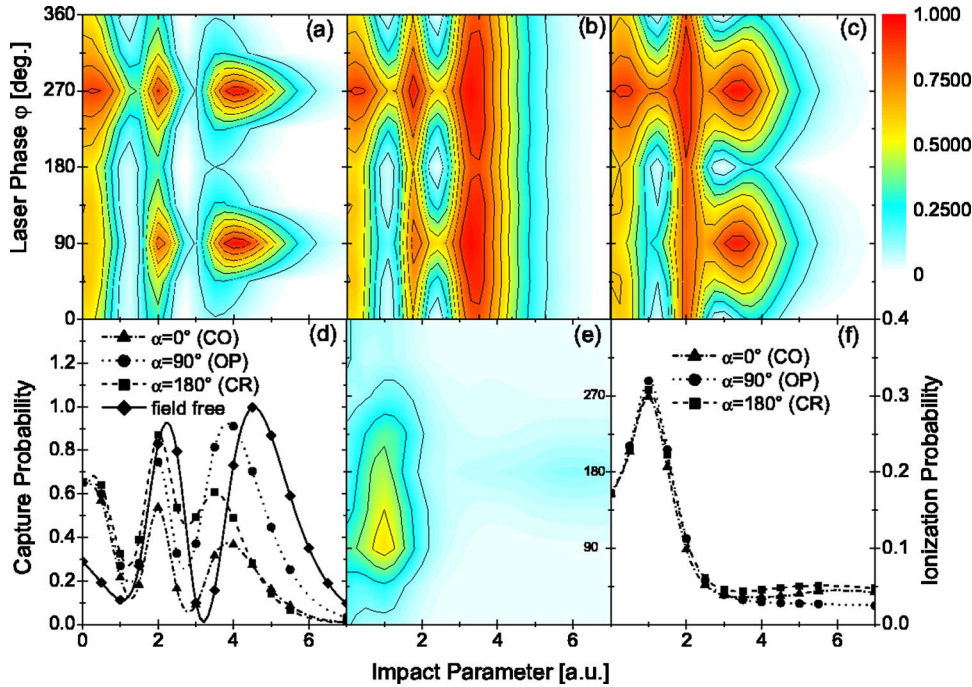
FIG. 3. (Color online) Contour plots of the electron capture probability (a)–(c) and the ionization probability (e) as a function of impact parameter and laser phase for corotating (CO) (a) and (e), off plane with $\alpha=\pm90°$ (OP) (b), and counterrotating (CR) (c) collisions. Also shown are the phase-averaged results for capture (d) and ionization (f), together with the field-free probabilities.

at laser phases of $\phi=90°$ and $\phi=270°$. The capture probability at $\phi=270°$ is slightly larger than at $\phi=90°$ due to stronger ionization in the latter case. Furthermore, the capture probability is enhanced for the counterrotating collision as compared to the corotating scenario. While for $b \leq 3$ the off-plane capture probability lies in general somewhere in between the corotating and counterrotating results, the electron capture probability at larger distances ($b>3$) becomes closer to the field-free value, and the laser-phase dependence nearly disappears [Fig. 3(b)].

Since the dependence on the laser phase ϕ cannot yet be controlled experimentally, we average the capture probability P_{cap} over all possible laser phases to obtain the phase-averaged capture probability,

$$\bar{P}_{\text{cap}}(b,\alpha) = \frac{1}{2\pi}\int_0^{2\pi} d\phi P_{\text{cap}}(b,\phi,\alpha), \tag{3}$$

shown in Fig. 3(d). For most impact parameters, the phase-averaged electron capture probability is larger for counterrotating than for corotating collisions, and noticeably smaller for field-free capture. For large impact parameters, the phase-averaged off-plane capture probabilities are closer to the field-free results than for both corotating and counterrotating collisions.

We found the dependence of capture and ionization probabilities on the impact angle to be rather smooth, such that no more than five different values $\alpha \in [0,180°]$ need to be evaluated for the integration over $bdbd\alpha$ to yield sufficiently accurate total cross sections. By limiting the range of impact-vector orientations, we partition the total capture cross section,

$$\sigma_{\text{cap}} = \int_{\alpha_{\min}}^{\alpha_{\max}} d\alpha \int_0^{\infty} dbb\bar{P}_{\text{cap}}(b,\alpha), \tag{4}$$

where $\alpha_{\min}=0°$, $\alpha_{\max}=360°$, into corotating and counterrotating contributions, $\sigma_{\text{cap}}^{\text{co}}$ and $\sigma_{\text{cap}}^{\text{counter}}$, by selecting

$\alpha_{\min}=-90°$, $\alpha_{\max}=90°$ and $\alpha_{\min}=90°$, $\alpha_{\max}=270°$, respectively. We find that the contribution of counterrotating collisions is larger by $|\sigma_{\text{cap}}^{\text{co}} - \sigma_{\text{cap}}^{\text{counter}}|/\sigma_{\text{cap}}=7.3\%$.

Table II shows total cross section from a previous two-dimensional model [8], which neglects all off-plane contributions. The second row of Table II includes results for the full three-dimensional calculation where, however, we only included projectile trajectories for fixed values of α (0°, 90°, and 180°, corresponding to corotating, off-plane, and counterrotating collisions). In both, the 2D model (first row) and the 3D model with fixed α (second row), we replaced the α-integration in (4) by a factor π, assuming isotropic capture for the entire half-space. Strikingly, for the reduced dimensionality model (first row), the integrated in-plane cross sections do not differ significantly from full dimensionality "fixed-α" cross sections (second row), where the projectile moves in the plane of the laser-electric field, i.e., where $\alpha=0°$ or 180° for corotating or counterrotating collisions, respectively. Thus for corotating and counterrotating collisions the two-dimensional model simulates three-dimensional results for trajectories with $\alpha=0°$ and 180° surprisingly well. A quantitative analysis, however, still requires the full three-dimensional calculation, i.e., the addition of off-plane trajectories (third row).

The ionization probability in Fig. 3(e) shows two main

TABLE II. Comparison of total laser-assisted capture cross sections for corotating, counterrotating, and off-plane collisions (see text).

	Corotating	Off-plane ($\alpha=90°$)	Counterrotating
2D model	26.2		43.7
3D (fixed α)	26.3	63.4	40.5
3D	44.9		51.9

features: (i) A maximum at $b \approx 1$ and a laser phase $\phi = 90°$, when the laser-electric field asserts an electric force on the electron in opposite direction to the projectile motion; and (ii) weak evidence for charge-resonant-enhanced ionization at $b \approx \pm 6$ and $\phi \approx 180°$ for corotating collisions [and a much broader and even weaker peak at $\phi \approx 0°$ for counterrotating collisions (not shown)]. After phase averaging, the ionization probability does not reveal a significant α dependence or dichroism effect, in contrast to the capture probability [Fig. 3(f)]. Interestingly, the enhancement of the ionization at the classical Bohr radius $b = 1$ is due to a combined effect of the collision and the laser field. The field-free ionization probability for $0 < b < 7$ is very small (below 0.07) and cannot be distinguished from zero on the scale of Fig. 3(f). Similarly, no significant ionization occurs for the interaction of the laser field with the target atom alone. However, due to the laser-electric field, the phase-averaged ionization probability increases dramatically and shows a pronounced maximum at $b = 1$. As a tentative explanation, we suggest a two-step process, where the collision promotes the electron into an excited target state, which subsequently gets ionized by absorbing a few photons from the laser field.

Summarizing, we have numerically solved the full three-dimensional time-dependent Schrödinger equation and have shown that a significant difference (dichroism) in the laser-assisted capture probability occurs for corotating and counterrotating collisions. We found a strong laser-phase dependence for both, capture and ionization, and weak evidence for a charge-resonant enhanced ionization process. We also found good agreement with previous two-dimensional model calculations, for the special case that the collision and the laser plane coincide. We hope that experimental data on laser-assisted collisions with controlled laser and collision parameters will soon confirm these predictions.

[1] T. Brabec and F. Krausz, Rev. Mod. Phys. **72**, 545 (2000).

[2] M. Protopapas, C. H. Keitel, and P. L. Knight, Rep. Prog. Phys. **60**, 389 (1997).

[3] C. J. Joachain, M. Dörr, and N. Kylstra, Adv. At., Mol., Opt. Phys. **42**, 225 (2000).

[4] J. H. Posthumus, Rep. Prog. Phys. **67**, 623 (2004).

[5] T. Kirchner, Phys. Rev. A **69**, 063412 (2004).

[6] S.-M. Li, J. Chen, and Z.-F. Zhou, J. Phys. B **35**, 557 (2002).

[7] M. S. Pindzola, T. Minami, and D. R. Schultz, Phys. Rev. A **68**, 013404 (2003).

[8] T. Niederhausen, B. Feuerstein, and U. Thumm, Phys. Rev. A **70**, 023408 (2004).

[9] A. B. Voitkiv and J. Ullrich, J. Phys. B **34**, 4383 (2001).

[10] L. B. Madsen, J. P. Hansen, and L. Kocbach, Phys. Rev. Lett. **89**, 093202 (2002).

[11] M. Lein and J. M. Rost, Phys. Rev. Lett. **91**, 243901 (2003).

[12] F. Ehlotzky, A. Jaroń, and J. Z. Kamiński, Phys. Rep. **297**, 63 (1998).

[13] C. Höhr, A. Dorn, B. Najjari, D. Fischer, C. D. Schröter, and J. Ullrich, Phys. Rev. Lett. **94**, 153201 (2005).

[14] H. J. Mason, Rep. Prog. Phys. **56**, 1275 (1993).

[15] R. Dörner, V. Mergel, O. Jagutzki, L. Spielberger, J. Ullrich, R. Moshammer, and H. Schmidt-Böcking, Phys. Rep. **330**, 95 (2000).

[16] J. Ullrich, R. Moshammer, A. Dorn, R. Dörner, L. P. H. Schmidt, and H. Schmidt-Böcking, Rep. Prog. Phys. **66**, 1463 (2003).

[17] C. L. Cocke (private communication).

[18] B. Feuerstein (private communication).

[19] G. Ferrante, L. L. Casico, and B. Spagnolo, J. Phys. B **14**, 3961 (1981).

[20] W. H. Press, B. P. Flannery, S. A. Teukolsky, and W. T. Vetterling, *Numerical Recipes in FORTRAN 77* (Cambridge University Press, Cambridge, England, 1992).

[21] U. Thumm, *Book of Invited Papers, XXII. ICPEAC, Santa Fe, NM* (Rinton, Princeton, NJ, 2002), p. 592.

[22] S. C. Cheng and B. D. Esry, Phys. Rev. A **72**, 022704 (2005).

[23] B. Feuerstein and U. Thumm, Phys. Rev. A **67**, 043405 (2003).

[24] M. W. Gealy and B. VanZyl, Phys. Rev. A **36**, 3091 (1987).

[25] B. J. Killian, R. Cabrera-Trujillo, E. Deumens, and Y. Öhrn, J. Phys. B **37**, 4733 (2004).